The Relationship Between Scleral Strain Change and Differential Cumulative Intraocular Pressure Exposure in the Nonhuman Primate Chronic Ocular Hypertension Model

Massimo A. Fazio,[1] Michael J. A. Girard,[2] Wonyul Lee,[3] Jeffrey S. Morris,[3] Claude F. Burgoyne,[4] and J. Crawford Downs[1]

[1]Department of Ophthalmology, University of Alabama at Birmingham, Birmingham, Alabama, United States
[2]In Vivo Biomechanics Laboratory, Department of Biomedical Engineering, National University of Singapore, Singapore
[3]Department of Biostatistics, The University of Texas MD Anderson Cancer Center, Houston, Texas, United States
[4]Optic Nerve Head Biomechanics Laboratory, Devers Eye Institute, Portland, Oregon, United States

Correspondence: J. Crawford Downs, Department of Ophthalmology and Visual Sciences, University of Alabama at Birmingham, 1670 University Boulevard, VH 390A, Birmingham, AL 35294, USA; cdowns@uabmc.edu.

Submitted: March 12, 2019
Accepted: August 17, 2019

Citation: Fazio MA, Girard MJA, Lee W, Morris JS, Burgoyne CF, Downs JC. The relationship between scleral strain change and differential cumulative intraocular pressure exposure in the nonhuman primate chronic ocular hypertension model. *Invest Ophthalmol Vis Sci*. 2019;60:4141–4150. https://doi.org/10.1167/iovs.19-27060

Purpose. To determine the relationship between peripapillary scleral strain change and cumulative differential IOP exposure in nonhuman primates (NHPs) with unilateral chronic ocular hypertension.

Methods. Posterior scleral shells from 6 bilaterally normal and 10 unilateral chronic ocular hypertension NHPs were pressurized from 5 to 45 mm Hg, and the resulting full-field, three-dimensional, scleral surface deformations were acquired using laser speckle interferometry. Scleral tensile strain (local tissue deformation) was calculated by analytical differentiation of the displacement field; zero strain was assumed at 5 mm Hg. Maximum principal strain was used to represent the scleral strain, and strains were averaged over a 15°-wide (~3.6-mm) circumpapillary region adjacent to the ONH. The relative difference in mean strain was calculated between fellow eyes and compared with the differential cumulative IOP exposure within NHPs during the study period. The relationship between the relative difference in scleral strain and the differential cumulative IOP exposure in fellow eyes was assessed using an *F* test and quadratic regression model.

Results. Relative differential scleral tensile strain was significantly associated with differential cumulative IOP exposure in contralateral eyes in the chronic ocular hypertension NHPs, with the bilaterally normal NHPs showing no significant strain difference between fellow eyes. The sclera in the chronic ocular hypertension eyes was more compliant than in their fellow eyes at low levels of differential cumulative IOP exposure, but stiffer at larger differential IOPs ($P < 0.0001$).

Conclusions. These cross-sectional findings suggest that longitudinal IOP-induced changes in scleral mechanical behavior are dependent on the magnitude of differential cumulative IOP exposure.

Keywords: nonhuman primate, biomechanics, sclera, ocular hypertension

Glaucoma is the second leading cause of blindness worldwide[1] and leads to irreversible vision loss through damage to retinal ganglion cell axons as they pass through the scleral canal at the optic nerve head (ONH).[2,3] Although glaucoma pathogenesis is not well understood, the biomechanical environment of the ONH has been hypothesized to play an important role in the neuropathy.[4–6] The sclera is an important factor in ONH biomechanics, and recent work strongly suggests that the biomechanics of the posterior sclera and lamina cribrosa are tightly coupled.[7–12] The sclera is the principal load-bearing tissue of the posterior pole, and provides the mechanical boundary conditions for the contained lamina cribrosa at its insertion into the scleral canal wall. Computational models have shown that scleral stiffness[10,12] and scleral collagen fiber organization[11,13] largely dictate the IOP-induced deformation exhibited by the ONH.

Sclera exhibits significant biomechanical changes with age,[14–17] race,[17,18] and glaucoma[15] in human eyes, and has been shown to exhibit altered material properties after exposure to chronic ocular hypertension in nonhuman primates (NHPs).[19] To investigate the influence of scleral biomechanics in the pathogenesis of glaucomatous damage, it is important to determine if the scleral mechanical response to IOP can be altered by prolonged exposure to elevated IOP. Remodeling-driven changes in scleral stresses and strains could lead to changes in scleral biomechanics and thus alterations in ONH biomechanics that precede the onset of glaucoma, and then change throughout disease progression to advanced disease. Hence, we focused this work on the differences in scleral strain that develop in the NHP model of unilateral chronic ocular hypertension, compared against untreated fellow eyes as an internal control, to investigate the changes

in scleral stiffness that may occur as a result of chronic exposure to elevated IOP. In addition, bilaterally normal NHPs that received no treatment in either eye were used as a naïve control group for physiologic intereye differences in scleral stiffness.

We have shown that NHPs exhibit significant alterations in the architecture of the laminar and peripapillary scleral connective tissues at the earliest stage of chronic ocular hypertension.[20–24] In the lamina cribrosa of chronic ocular hypertension NHP eyes, permanent deformation and thickening,[23,24] accompanied by increases in both total connective tissue volume and total number of laminar beams through the thickness of the lamina, were observed.[22] In addition, we observed posterior laminar deformation and progressive posterior migration of the laminar insertion, accompanied by thinning in the peripapillary and posterior sclera in the chronic ocular hypertension eyes.[23,25] In vivo, several NHP studies have shown that the ONH and peripapillary connective tissues change in both structural stiffness and morphology very early in chronic ocular hypertension.[26–29] These morphologic changes suggest rapid and significant change in ONH structure due to elevated IOP exposure and are likely the result of connective tissue remodeling in response to chronically elevated stress and strain levels.[30]

We have previously shown that the biomechanical properties of the peripapillary sclera are altered in early chronic ocular hypertension using uniaxial testing of scleral strips and linear viscoelastic theory.[31] That study demonstrated a significant increase in the equilibrium modulus of the peripapillary sclera from chronic ocular hypertension NHP eyes, but no changes were seen in the time-dependent viscoelastic parameters. We have also shown that the peripapillary sclera thins significantly in response to chronic exposure to elevated IOP in NHPs using histomorphometry.[23]

In a more recent study, we used posterior pole inflation testing in eight NHPs with unilateral early chronic ocular hypertension, and back-fit scleral material properties to study the differences in scleral tangent modulus between fellow glaucomatous and control eyes.[19] In that study, scleral material properties in eyes with chronic ocular hypertension were significantly altered compared to their fellow control eyes in most animals. The reported changes were animal specific and the material property differences were isolated to those early chronic ocular hypertension eyes that experienced either lower IOPs ($\leq$30 mm Hg) and smaller cumulative IOP differences, or higher IOPs ($\geq$30 mm Hg) and larger cumulative IOP differences. Results showed that scleral remodeling was a common feature of chronic exposure to elevated IOP, but the response was eye specific. This study did not include either bilaterally normal NHPs as controls, or NHPs with severe chronic ocular hypertension that corresponded to higher levels and/or longer durations of elevated IOP exposure. The structural response of the scleral shell to IOP (deformation or strain) is determined by both scleral shell geometry (thickness, shape) and material properties (material stiffness of scleral tissue). Scleral structural response is best quantified in terms of tissue strain, which is the relative local deformation (stretch, compression, shear, or a combination) expressed as a percentage change from baseline. However, our previous studies of scleral biomechanics in NHP chronic ocular hypertension eyes have not reported strain.

We recently developed a method to calculate continuous strain maps from three-dimensional (3D) scleral surface deformations measured on posterior scleral shells subjected to inflation testing.[32,33] This advance allows the investigation of differences in strain in chronic ocular hypertension eyes versus fellow control eyes as a function of the level of exposure to elevated IOP using an accurate and validated measurement technique. In the present study, we calculated scleral strain maps by reanalyzing the scleral deformation data from six of the eight animals of our previously published report on scleral material property changes with exposure to mild and moderate levels of differential cumulative IOP exposure (elevated IOP in one eye compared to the fellow control).[19] We then added data from four additional animals with severe levels of differential cumulative IOP exposure to expand the IOP exposure range of the study cohort. Finally, we added scleral strain measurements from six bilaterally normal NHPs to establish the range of intraeye differences in scleral stiffness among normal fellow eyes. The purpose of this study was to determine if there is a relationship between scleral strain and the differential cumulative IOP exposure in treated versus fellow control eyes in the unilateral NHP chronic ocular hypertension model.

Materials and Methods

All experiments adhered to the ARVO Statement for the Use of Animals in Ophthalmic and Vision Research, and were performed with approval from the Legacy Health Institutional Animal Care and Use Committee.

A control group of six bilaterally normal NHPs was used to establish baseline variability in scleral structural stiffness between normal fellow eyes. Elevated IOP was induced in one eye of the treated group of 10 NHPs by photocoagulating the trabecular meshwork, while the fellow eye was used as a control. Data from only six of the eight animals from our previous study were included in this analysis, as the strain calculation technique we employed requires very small deformation steps to ensure accurate strain quantification; deformation steps were too large in at least one eye of two NHPs studied previously, so these data were deemed unreliable and excluded from this analysis. Four additional NHPs with late-stage chronic ocular hypertension were included in addition to the 6 NHPs with early to moderate chronic ocular hypertension that we reported previously, for a total of 10 NHPs with unilateral chronic ocular hypertension and 6 bilaterally normal NHPs.

The protocol for generating and detecting laser-induced elevated IOP, or chronic ocular hypertension, has been fully described in previous reports.[21,34,35] Briefly, both eyes of each animal underwent IOP measurement (Tonopen XL; Reichert, Depew, NY, USA) and confocal scanning laser tomographic (CSLT) and spectral-domain optical coherence tomography (SD-OCT) imaging (Heidelberg Retinal Tomograph and Spectralis; Heidelberg Engineering, Heidelberg, Germany) at a manometer-controlled IOP of 10 mm Hg on three to five occasions while normal to establish baseline variability. Imaging was performed every 1 to 2 weeks after laser photocoagulation of the trabecular meshwork (OcuLight TX; Iridex, Mountain View, CA, USA) and chronic IOP elevation in one eye, until the onset and/or progression of CSLT-detected ONH surface change of mean position of the disc (MPD) or HRT II topographic change analysis (TCA).[36] NHPs used in this study were euthanized at varying levels of glaucomatous damage as assessed by confocal scanning laser ophthalmoscope-measured ONH surface change, or MPD, ranging from the earliest detectable MPD change in three NHPs to severe disease in which MPD did not change further even after additional exposure to elevated IOP in four NHPs. This clinical measure of ONH surface topography change in the glaucoma eye covered a wide range of glaucoma severity, and yielded a wide range of differential cumulative IOP exposure in fellow eyes. All animals were euthanized under ketamine/xylazine anesthesia with an intravenous injection of pentobarbital

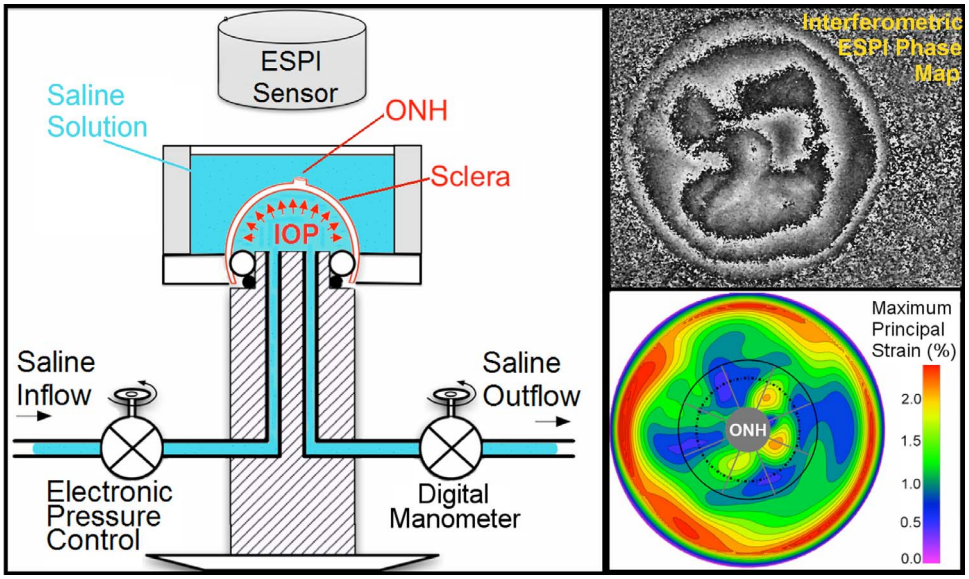

Figure 1. Diagram of the inflation testing apparatus (*left*). *Upper right*: a typical correlation fringe pattern representing the laser waveform phase variation measured by the ESPI. *Lower right*: a typical maximum principal strain map of the outer surface of the posterior sclera, showing the boundary of the 15°-wide region surrounding the ONH that was assessed in this study. Note that a *dashed line* denotes the external boundary of the peripapillary region (~2.2 mm wide) and the *solid gray line* denotes the external boundary of the midposterior region (defined such that it has the same surface area as peripapillary region). Figure reprinted with permission from Fazio et al.[18]

sodium, and their eyes were enucleated immediately post mortem for scleral inflation testing.

Scleral Mechanical Testing, and Definition of the Mechanical Strain

The experimental protocol for inflation testing the posterior scleral shell has been fully described in our previous reports.[14,16,19,33] Briefly, the posterior scleral shells were cleaned of intra- and extraorbital tissues immediately post mortem, and individually mounted on a custom-built pressurization apparatus (Fig. 1, left). Each eye was blotted dry, covered with a white contrast medium (ProCAD Contrast Medium; Ivoclar, Schaan, Lichtenstein), and then immediately immersed in PBS at room temperature (Fig. 1, left). Preconditioning loads were applied in the form of 20 pressurization cycles from 5 to 30 mm Hg at a rate of 5 mm Hg per second, and then the scleral shell was allowed to recover for 15 minutes. A starting pressure of zero could not be used because the posterior scleral shell of NHPs does not maintain its shape unless pressurized to at least 2 mm Hg and exhibits geometric nonlinearities up to 4 mm Hg, so a starting pressure of 5 mm Hg was used. The scleral shells were inflated from 5 to 45 mm Hg in small steps of 0.01 to 0.2 mm Hg using an automated system with computer feedback control. Scleral surface displacements were recorded after the sclera had reached equilibrium at each pressure step (~30 seconds) using a commercial electronic laser speckle interferometer (ESPI; Q-100, Dantec Dynamics A/S, Skovlunde, Denmark) (Fig. 1; right, top). In a recent study, we assessed the displacement measurement uncertainty of this ESPI system in inflation testing conditions similar to those used herein, and the average measurement uncertainty was ±16 nm at the 95% confidence level.[32] As in previous studies (Fazio MA, et al. *IOVS* 2014;55:ARVO E-Abstract 4552),[14,16,19,33] all inflation testing was performed at room temperature to avoid artifacts from convection currents in the saline bath that interfere with the laser displacement measurements.

A customized B-spline fitting system[37] was used to obtain continuous and differentiable analytical functions that define the 3D displacement field over the entire posterior third of the scleral surface as described previously.[33] The 3D deformation of the infinitesimally thin outer layer of the sclera was obtained by analytical differentiation of the fitting system functions, which allows direct calculation of the mechanical strain without any intermediate finite element or analytical modeling. The strain formulation is reported in Equations 1 and 2, as described in our previous studies,[16,18,33] and the 3D strain tensor was computed using an approximated formulation as follows:

ESPI displacements in Cartesian space were fit to continuous, differentiable, analytical functions $\cup(\theta,\varphi) = \{u_\theta(\theta,\varphi), u_\varphi(\theta,\varphi), u_r(\theta,\varphi)\}$ for the meridional $\theta \in [0,\frac{\pi}{2}]$, circumferential $\varphi \in [0,2\pi]$, and radial directions, respectively. The analytical function defines the displacement field over the two-thirds of the outer surface of the posterior pole of each eye. Five ($\varepsilon_{\theta\theta},\varepsilon_{\theta\varphi},\varepsilon_{\varphi\varphi},\varepsilon_{r\varphi},\varepsilon_{r\theta}$) out of nine components of the full strain tensor (Equation 1) were computed by direct mathematical differentiation of the analytical displacement functions, and by assuming that the displacement components tangent to the scleral surface do not vary in the radial direction. A recent study by Tang and Liu[38] showed that variation of the meridional and circumferential components of displacement in the radial direction is minimal in the infinitesimally thin outer layer of the sclera where strain was calculated in this study. So, meridional and circumferential displacement variation in the radial direction, $\frac{\partial u_\theta}{\partial r}(\theta,\varphi)$ and $\frac{\partial u_\varphi}{\partial r}(\theta,\varphi)$ in Equation 2, respectively, was assumed to be zero, and the sensitivity of the reported outcomes to this assumption was quantified and reported to be very low in our previous study.[16]

Three components of the strain tensor $\varepsilon_{\varphi\theta}$, $\varepsilon_{\theta r}$, and $\varepsilon_{\varphi r}$ were computed by strain compatibility equations, and the final component, ε_{rr}, was numerically computed by assuming tissue incompressibility, thereby imposing $det[\varepsilon + I] = 1$ (where I is the Identity Matrix).

$$\text{Strain Tensor} = \varepsilon(\theta,\varphi) = \begin{Bmatrix} \varepsilon_{\theta\theta} & \varepsilon_{\theta\varphi} & \varepsilon_{\theta r} \\ \varepsilon_{\varphi\theta} & \varepsilon_{\varphi\varphi} & \varepsilon_{\varphi r} \\ \varepsilon_{r\theta} & \varepsilon_{r\varphi} & \varepsilon_{rr} \end{Bmatrix}, \quad (1)$$

where

$$\begin{cases} \varepsilon_{\theta\theta} = \frac{1}{r}\left(\frac{\partial u_\theta}{\partial\theta} + u_r\right) \\ \varepsilon_{\varphi\varphi} = \frac{1}{r\sin\theta}\left(\frac{\partial u_\varphi}{\partial\varphi} + u_r\sin\theta + u_\theta\cos\theta\right) \\ \varepsilon_{\theta\varphi} = \frac{1}{2r}\left(\frac{1}{\sin\theta}\frac{\partial u_\theta}{\partial\varphi} + \frac{\partial u_\varphi}{\partial\theta} - u_\varphi\cot\theta\right) \\ \varepsilon_{r\theta} = \frac{1}{2}\left(\frac{1}{r}\frac{\partial u_r}{\partial\theta} + \frac{\partial u_\theta}{\partial r} - \frac{u_\theta}{r}\right) \\ \varepsilon_{r\varphi} = \frac{1}{2}\left(\frac{1}{r\sin\theta}\frac{\partial u_r}{\partial\varphi} + \frac{\partial u_\varphi}{\partial r} - \frac{u_\varphi}{r}\right) \end{cases} \quad (2)$$

The maximum principal tensile strain (ε_I, Equation 3) was computed over the entire scleral surface from the spectral decomposition of the full strain tensor:

$$\varepsilon^{Eig} = \begin{Bmatrix} \varepsilon_I & 0 & 0 \\ 0 & \varepsilon_{II} & 0 \\ 0 & 0 & \varepsilon_{III} \end{Bmatrix} \quad (3)$$

The radius of the spherical coordinate system was computed by best-fitting 3D coordinates of ~2500 points on the outer surface of the posterior sclera. These points were acquired using a 3D digitizer with a nominal resolution of ~200 μm (MicroScribe G2X, Immersion; San Jose, CA, USA), while the sclera was pressurized to 10 mm Hg with PBS. A pressure of 10 mm Hg was chosen to reduce the potential for deformation of the sclera with the digitizer tip so as to get the best possible scleral surface geometries. The difference in shape of the sclera when pressurized at 10 mm Hg compared to 5 mm Hg is negligible as compared to the intrinsic 200-μm resolution of the digitizer. Also, while the strain is a function of the radius of the sphere defining the coordinate system, the sensitivity of the strain to an error in the sphere radius is negligible.[16]

Error Assessments and Sensitivity Analysis

As reported in detail in our previous study,[16] we showed that the all sources of error and approximation combined would produce maximum relative principal strain error below 3.8%, which is negligible given the differences in the relative strain results reported herein.

Relative Strain Difference, and Differential Cumulative IOP

The load-bearing connective tissues of the posterior sclera experience elevated IOP directly,[4] whereas they are likely to be only minimally affected by glaucomatous alterations to the neural and connective tissues of the ONH. In order to minimize the influence of structural and morphologic parameters on scleral strain, we used differential average maximum principal (tensile) strain and the differential cumulative IOP exposure between fellow eyes of the same animal. Accordingly, we refer to the relative difference in average tensile strain according to the formula:

$$\text{Relative Strain Difference} = (Strain_{treated} - Strain_{control})/(Strain_{treated} + Strain_{control}), \quad (4)$$

where treated and control denote the lasered eye with elevated IOP and the normal fellow eye, respectively.

This formulation allows for quantification of the relative difference in magnitude of the scleral strain between fellow eyes from the same animal. To quantify the relative strain between fellow eyes from the bilaterally normal control group (six NHPs), the eyes were randomly assigned to the treated and control groups for the purposes of calculating relative strain difference in Equation 4 and differential cumulative IOP in Equation 5, even though both eyes are untreated. These assignments were randomly permutated 64 times in the statistical analysis to ensure that the physiologic differences between normal eyes did not bias the results.

In order to assess the strain difference as a function of the exposure to elevated IOP in the treated eye, we computed the difference in the cumulative IOP (CumIOP) between the treated and control eyes within each NHP as:

$$\text{Differential Cumulative IOP} = \delta\text{CumIOP} = \text{CumIOP}_{\text{treated}} - \text{CumIOP}_{\text{control}}. \quad (5)$$

Cumulative IOP for a given eye is defined as the area under its IOP over time curve—computed using a trapezoidal numerical integration (Fig. 2)—which provides a concise quantification of how much time a given eye has been exposed to a given IOP. Again, the fellow eyes from the bilateral normal NHPs were randomly assigned to either the treated and control groups for the purposes of strain and differential IOP calculations in Equations 4 and 5 so we could assess physiologic differences between normal eyes, even though there was no treated eye in these animals. These assignments were randomly permutated 64 times in the statistical analysis to ensure that the physiologic differences between normal eyes did not bias the results.

Statistical Analysis: The Nonlinear Relationship Between Relative Strain Difference Versus Differential Cumulative IOP

An F test can be performed to determine if the quadratic relationship fits the relationship between relative strain difference and differential cumulative IOP in the combined normal and treated data better than a linear relationship,

$$\text{Linear Model}: Y = \beta_0 + \beta_1 X + \varepsilon$$

$$\text{Quadratic Model}: Y = \beta_0 + \beta_1 X + \beta_2 X^2 + \varepsilon, \quad (6)$$

where Y is the relative strain difference and X is the differential cumulative IOP.

Under the null hypothesis that the quadratic model does not provide a significantly better fit than the linear model, the F statistic has an F distribution with (1,13) degrees of freedom. We can reject the null hypothesis with a small P value. The problem here is that control and treated assignments in the bilaterally normal control group ($n = 6$) are arbitrary. To deal with this issue, we counted how many times we rejected the null hypothesis over all possible $2^6 = 64$ combinations of labels in the control group (each F test is rejected if the corresponding P value is less than 0.01).

To assess statistical significance of the quadratic relationship, the following null model of no association is tested against the quadratic model in Equation 6 above:

$$\text{Null Model}: Y = \beta_0 + \varepsilon.$$

An F statistic can be obtained to compare the null model and the quadratic model. As the labels in the bilaterally normal control group are arbitrary, the average of the F statistic over all combinations of control labels in the control group is computed. Since it is averaged over all possible combinations of labels in the control group, it no longer has an F distribution.

Investigative Ophthalmology & Visual Science

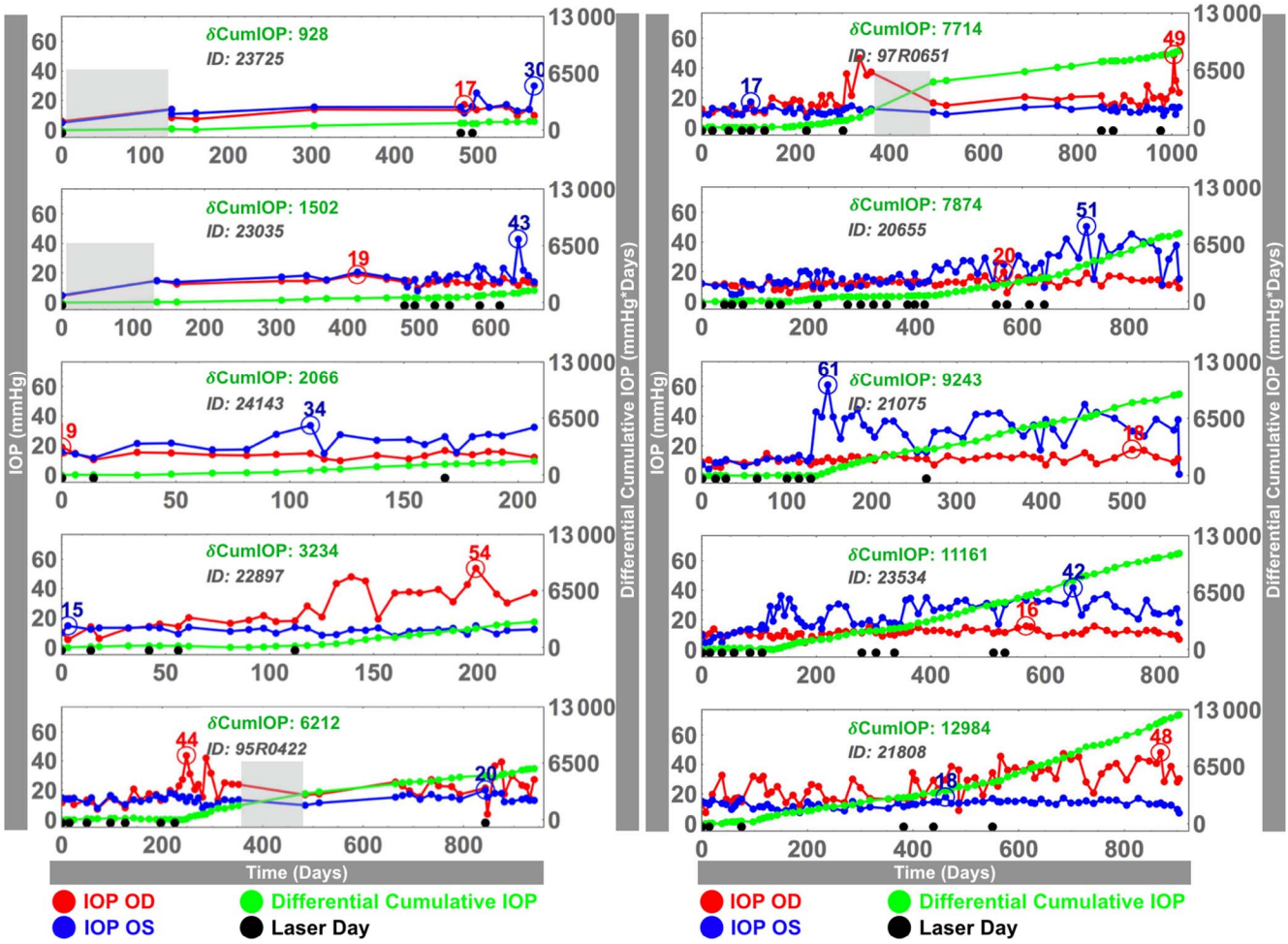

Figure 2. Postlaser IOP histories in both eyes (*blue*, *red*) of the 10 chronic ocular hypertension NHPs in this study. For each animal, time 0 corresponds to the first laser session, and the last day is the date of euthanasia; note that time scales are different for each animal. *Black dots* along the *x*-axis signify each laser session. For each NHP, differential cumulative IOP (*green curve* in mm Hg·days; scale at *right*) was defined as the difference in area under the IOP versus time curve between the lasered and the normal eyes. Maximum detected IOP in each eye is shown with an *open circle*. *Shaded gray area*: August 30, 2005 to December 15, 2005; represents the period immediately after Hurricane Katrina, during which IOP could not be measured in some NHPs; see the Limitations section of the Discussion.

In order to calculate a P value of the averaged F statistic, we perform a permutation test in which the relative strain differences (Y) are permuted within the glaucoma group so that the relationship between X and Y is uncoupled. Permuted data sets can be considered as data sets from the null of no association between X and Y. By computing the averaged F statistic for each permuted data set, we can have a sampling distribution under the null hypothesis that the differential cumulative IOP has no effect on the relative strain difference. A final P value can be calculated using the proportion of computed average F statistic values from permuted data sets that are larger than the average test statistic value from the original data set.

Results

Table 1 shows the relevant demographic information for the NHPs used in this study, including the relative strain difference in fellow eyes. Note that the bilateral normal eyes have relative strain differences of both positive and negative values, reflecting the fact that they do not have a treated eye; hence the relative strain difference as calculated in Equation 4 was performed with both the left and right eyes assigned to the

Table 1. Demographic, Treatment, and Relative Strain Difference in the Posterior Sclera (Both Regions Combined) Between Fellow Eyes for All NHPs

Animal ID	Treatment	Age, Years	Relative Strain Difference
25108	Normal	1.6	±0.00
24866	Normal	18	±0.01
25128	Normal	1.6	±0.02
109	Normal	30	±0.08
23578	Normal	20	±0.08
24448	Normal	23	±0.11
21808	COH	10	−0.60
23534	COH	12	−0.29
23035	COH	23	−0.08
23725	COH	23	−0.08
22897	COH	21	−0.03
97R0651	COH	10	0.00
24143	COH	19	0.11
95R0422	COH	12	0.16
20655	COH	11	0.17
21075	COH	10	0.17

COH, chronic ocular hypertension.

Table 2. The Number of Rejections in *F* Test for Determining the Optimal Regression Model Describing the Relative Strain Difference as a Function of the Differential Cumulative IOP

Region	Number of Times the Quadratic Model Was a Better Fit (Out of 64)
Peripapillary, PP	64
Midperipheral, MP	18
PP + MP	64

treated group in succession as a means to assess the physiologic differences between fellow normal eyes.

The analysis of the *F* statistic obtained from the 64 permutations of the control and treated labels of the normal group (six pairs) showed that the quadratic regression model (Equation 6) fit the relative strain variation over differential cumulative IOP significantly better than a linear model for the peripapillary region (Table 2; Fig. 3). For the midperipheral region alone, the quadratic regression model is not a better fit (Table 2; Fig. 3, right). When the overall responses of the peripapillary and midperipheral regions are combined, the quadratic model was significantly better for all the possible 64 combinations, meaning that the overall relative strain difference with differential cumulative IOP for both regions together is better described by a quadratic relationship.

After assessing which regression model better describes the evolution of the relative strain difference as a function of differential cumulative IOP, and by computing the averaged *F* statistic for each permuted data set as described above, a final *P* value can be computed for testing the statistical significance of this functional relationship (Table 3).

For the peripapillary and midperipheral regions, the relative strain difference significantly changed with differential cumulative IOP ($P = 0.0024$ and 0.0279, respectively, Table 3). Also, the overall relative strain difference within the posterior sclera (both regions combined) changed significantly with differential cumulative IOP ($P = 0.0067$, Table 3).

Relative strain difference had no significant correlation with age, mean measured IOP, or maximum measured IOP.

Discussion

These results show that strain differences in fellow eyes are related to the level of chronic IOP elevation, and the resulting mechanical behavior is dependent on the differential cumulative IOP exposure over time (a dose effect). Eyes with progressively higher differential cumulative IOP exposures demonstrated significantly greater compliance compared to their fellow control eyes up to approximately 6000 mm Hg·days, manifesting as progressively increasing scleral tensile strain differences that peaked at ~28% (Fig. 3). Eyes with cumulative IOP exposures greater than 10,000 mm Hg·days higher than their fellow control eyes demonstrated significantly lower strains than their fellow control eye (Fig. 3). The relationship was more pronounced in the peripapillary sclera than the midperipheral sclera farther away from the ONH. Taken together, these cross-sectional data predict the trajectory of longitudinal, eye-specific, scleral strain change within individual NHP eyes after chronic IOP elevation.

Significant changes in strain were observed in NHPs beginning at approximately 4000 to 6000 mm Hg·days of differential cumulative IOP in the treated eye (Fig. 3). Prior to this level of differential IOP exposure, no effect is apparent, which suggests that the sclera and its resident cells are somewhat tolerant of mild cumulative elevations in IOP. Several studies have reported that mechanical strain applied to scleral fibroblasts triggers the release of matrix metalloproteinases (MMPs) and suppresses release of MMP inhibitors, which can then lead to remodeling of the scleral extracellular matrix.[39,40] While we did not measure cellular responses, it is plausible that scleral fibroblasts become more active at higher strain levels and increase remodeling of the scleral extracellular matrix (ECM). Our results suggest that the remodeling process follows a classic connective tissue wound healing response, in which the sclera breaks down and becomes more compliant initially as it reorganizes, followed by a scarring period in which the sclera progressively stiffens as the collagen consolidates, eventually resulting in the significant stiffening of the sclera even relative to the normal level prior to injury.

This agrees with our previous study of a subset of these animals, in which we observed significant changes in scleral tangent modulus between the normal and glaucomatous eyes of NHPs.[19] Also, Burgoyne and colleagues[28,41] reported hypercompliance of the ONH surface, lamina cribrosa, and

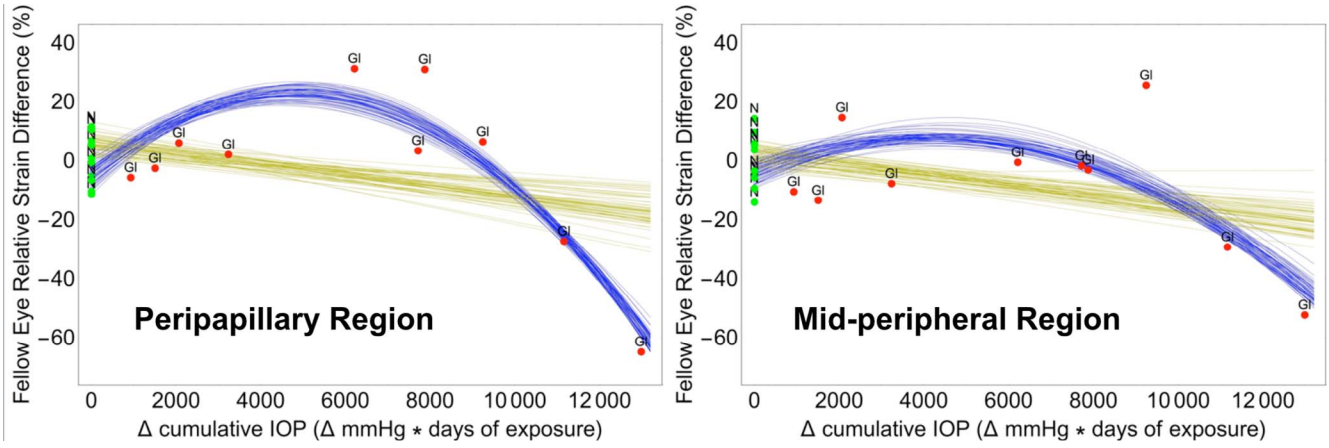

Figure 3. Linear (*gold*) and nonlinear (quadratic, *blue*) statistical models showing the significant relationship between relative strain difference and differential cumulative IOP exposure between fellow eyes within NHPs in the peripapillary sclera within 2.2 mm of the scleral canal opening and the midperipheral sclera farther away from the ONH. N, bilaterally normal NHPs (*green*); GI, NHPs in which one eye was exposed to chronic ocular hypertension (*red*).

Table 3. Averaged *F* Statistic Over All Possible Combinations and Its Permutation *P* Value for the Relative Strain Difference as a Function of the Differential Cumulative IOP

Region	Averaged *F* Test Statistic	Permutation *P* Value
Peripapillary, PP	20.786	0.0024
Midperipheral, MP	6.272	0.0279
PP + MP	15.958	0.0067

peripapillary sclera using in vivo imaging within 4 to 8 weeks of chronic IOP elevation in NHPs and suggested that weakening of the load-bearing structures of the ONH through connective tissue damage might be responsible for this phenomenon at the earliest stage of chronic ocular hypertension. The latter study also noted stiffening of the lamina cribrosa in eyes exposed to longer-term chronically elevated IOP, as well as in optic nerve transection eyes.[28] Together, these studies showed that the ONH exhibits initial hypercompliance shortly after IOP elevation, followed by reduced compliance after long periods of chronically elevated IOP exposure, which mirrors the scleral results reported herein. In addition, our results suggest that the compliance changes are more pronounced in the peripapillary region, which is also consistent with prior studies. A separate computational modeling study also predicted a decrease in the elastic modulus, or stiffness, of the lamina cribrosa connective tissues at the earliest stage of chronic ocular hypertension in NHPs, based on lower stresses due to the increase in laminar connective tissue volume, but no decrease in laminar strain.[22,42]

The profile of the scleral functional remodeling response reported herein has been observed in other tissues and in vitro. In vivo tendon stiffening has been reported in functional human studies after prolonged periods of exercise and/or sporting activities that result in joint strain, which is consistent with the IOP-driven scleral stiffening results reported herein.[43–46] Previous studies in vitro have shown that collagen fibrils synthesize along the direction of applied strain,[47,48] and strained fibrils resist enzymatic degradation much better than unstrained fibrils.[49–53] These results support the notion that strained collagenous tissues respond to strain by adding new collagen fibrils and resisting natural collagen degradation.[54] Quigley et al.[55,56] and Hernandez and colleagues[57–59] described elastin disruption within the lamina cribrosa of both NHP and human glaucoma eyes with more advanced disease, accompanied by marked increase in collagen fibril density. However, none of the aforementioned studies were designed to detect the initial hypercompliant phase in tissues or collagen fibrils reported herein, as all subjects/specimens were subjected to similar levels of increased strain and measurements were made at baseline and study endpoint. It should be noted that this study assessed strain resulting from an IOP increase from 5 to 45 mm Hg, hence ignores the lower strain levels at which elastin response is likely to be an important contributor to scleral stiffness.

We hypothesize that initial scleral hypercompliance, followed by scleral stiffening in response to prolonged exposure to chronic IOP elevations shown herein, is an effort by the scleral fibroblasts to maintain the biomechanical homeostasis of the scleral shell through collagen fibril remodeling, which will be investigated in future studies. Figure 3 suggests that there is a window of scleral hypercompliance associated with increased strain in the peripapillary sclera, prior to the profibrotic response that strengthens the scleral structure to a level above the initial structural stiffness of the tissue prior to chronic IOP elevation. Surprisingly, the argument that a stiff scleral shell shields the ONH from glaucomatous damage[60] seems to contradict previous results showing that the sclera stiffens with age in both NHPs and humans,[14–17] with greater stiffening with age in persons of African heritage,[17,18] and elderly persons and individuals of African descent are more susceptible to glaucoma at all levels of IOP and all levels of RGC axon loss.[61–63] In addition, previous work in the murine model of glaucoma suggests that a stiffer sclera is associated with increased axon loss.[64,65]

However, the observed window of scleral hypercompliance at the onset of chronic ocular hypertension in NHPs prior to stiffening later in the disease process can serve to reconcile these conflicting observations, as the initial cascade of glaucomatous damage to the ONH may be initiated during this hypercompliant phase before the sclera and lamina can stiffen in response to mechanical strain insult. It is plausible that this stiffening phase occurs much later in the disease process, and after significant damage to the axons has manifested. It is also plausible that this later-phase scleral stiffening serves to increase the magnitude of IOP transients in the eye,[66–68] which could independently contribute to glaucomatous damage in addition to mean IOP, thereby failing to rescue the remaining axons and contributing to increased rates of disease progression in an already damaged eye.

Limitations

First, reporting a single strain value or ratio for the sclera does not adequately represent its biomechanical response. The different contributions of scleral anisotropy, hyperelasticity, and local variations in material properties and strain were not considered, and could provide further insight into the relationship between scleral biomechanics and axonal loss in glaucoma.

Although the general limitations of the method have been discussed at length in our previous reports,[14,16,33,69,70] we will briefly revisit them herein and then discuss those inherent to this study in particular. First, IOP was measured in both eyes of each NHP over time (Fig. 1), but we did not characterize daily IOP fluctuations that are known to exist in NHPs.[71,72] Diurnal IOP fluctuations have been shown to be large in NHPs, especially in glaucomatous eyes, in which they are highly eye specific and can exceed 10 mm Hg.[71] Therefore, our definition of cumulative IOP insult (change in area under the IOP versus time curve) was used here only to provide an estimate of the true cumulative insult from IOP. We have developed an implantable telemetric IOP transducer that is currently being used in NHPs that allows for continuous measurements of IOP fluctuations and very accurate characterization of IOP exposure.[66,68,73] In future studies, data from NHPs with well-characterized IOP insults will allow for more accurate characterization of the interactions between IOP and scleral and laminar remodeling.

Second, we did not characterize scleral biomechanics between 0 and 5 mm Hg in the tested eyes, because the scleral shells required an IOP of approximately 4 mm Hg to sustain their shape. IOPs in the range of 0 to 5 mm Hg are rarely measured in NHPs, and so ignoring the initial IOP loading should not compromise the integrity or importance of our results.

Finally, 9 of the 14 NHPs began this study while the investigators' laboratories were still located at the LSU Eye Center in New Orleans, and were unavailable for study for approximately 3 months after Hurricane Katrina. At the time of the hurricane, five of these nine NHPs had not yet been lasered, which includes three of the bilaterally normal NHPs and two of the chronic ocular hypertension NHPs, and so the

frequency of IOP measurement and assessment of pre- and postlaser cumulative IOP exposure in these animals was unaffected. However, four of these nine animals had already undergone initial laser, and so the accuracy of their cumulative IOP exposure calculations is affected by the lack of IOP data in that time span and the diminished frequency of testing after their arrival at Devers Eye Institute. During this time, cumulative IOP was calculated as described above, but the frequency of IOP measurement was sparse and therefore we assumed that IOP changed linearly between the last prehurricane measurement and the first measurement after the storm. This period was approximately 3 months in length (gray boxes shown in Fig. 2), and so unmeasured IOP changes during this period could induce errors in the cumulative IOP calculations in these NHPs. IOPs measured at the last prehurricane exam and the first posthurricane exam were very similar in all but one NHP (95R0651; Fig. 2) The remaining seven NHPs in the study were acquired at Devers and were altogether unaffected by these events.

Conclusions

These cross-sectional data suggest that changes in peripapillary and midperipheral scleral stiffness occur in response to chronic IOP elevation and that the resulting change in scleral mechanical behavior is dependent on the differential cumulative IOP exposure over time (a dose effect). The results of this cross-sectional study suggest that in eyes followed longitudinally, the sclera in the glaucoma eye will soften initially, resulting in temporarily higher scleral tensile strains as differential cumulative IOP exposure increases, but then will stiffen significantly thereafter to exhibit lower mean tensile strains. Currently, ex vivo inflation testing is the only feasible method for obtaining accurate measurements of scleral strain, and the results of this study demonstrate the need for the development of in vivo methods to evaluate scleral biomechanics longitudinally in NHPs and human subjects.

Acknowledgments

Supported by National Institutes of Health Grants R01-EY011610 (CFB), R01-CA107304 (JSM), R01-CA178744 (JSM); Eyesight Foundation of Alabama; Research to Prevent Blindness. The authors alone are responsible for the content and writing of the paper.

Disclosure: **M.A. Fazio**, None; **M.J.A. Girard**, None; **W. Lee**, None; **J.S. Morris**, None; **C.F. Burgoyne**, None; **J.C. Downs**, None

References

1. Quigley HA, Broman AT. The number of people with glaucoma worldwide in 2010 and 2020. *Br J Ophthalmol*. 2006;90:262–267.
2. Nickells RW, Howell GR, Soto I, John SW. Under pressure: cellular and molecular responses during glaucoma, a common neurodegeneration with axonopathy. *Annu Rev Neurosci*. 2012;35:153–179.
3. Howell GR, Libby RT, Jakobs TC, et al. Axons of retinal ganglion cells are insulted in the optic nerve early in DBA/2J glaucoma. *J Cell Biol*. 2007;179:1523–1537.
4. Burgoyne CF, Downs JC, Bellezza AJ, Suh JK, Hart RT. The optic nerve head as a biomechanical structure: a new paradigm for understanding the role of IOP-related stress and strain in the pathophysiology of glaucomatous optic nerve head damage. *Prog Retin Eye Res*. 2005;24:39–73.
5. Downs JC. Optic nerve head biomechanics in aging and disease. *Exp Eye Res*. 2015;133:19–29.
6. Campbell IC, Coudrillier B, Ross Ethier C. Biomechanics of the posterior eye: a critical role in health and disease. *J Biomech Eng*. 2014;136:021005.
7. Bellezza AJ, Hart RT, Burgoyne CF. The optic nerve head as a biomechanical structure: initial finite element modeling. *Invest Ophthalmol Vis Sci*. 2000;41:2991–3000.
8. Sigal IA, Flanagan JG, Ethier CR. Factors influencing optic nerve head biomechanics. *Invest Ophthalmol Vis Sci*. 2005;46:4189–4199.
9. Norman RE, Flanagan JG, Sigal IA, Rausch SM, Tertinegg I, Ethier CR. Finite element modeling of the human sclera: influence on optic nerve head biomechanics and connections with glaucoma. *Exp Eye Res*. 2011;93:4–12.
10. Sigal IA, Yang H, Roberts MD, et al. IOP-induced lamina cribrosa deformation and scleral canal expansion: independent or related? *Invest Ophthalmol Vis Sci*. 2011;52:9023–9032.
11. Coudrillier B, Boote C, Quigley HA, Nguyen TD. Scleral anisotropy and its effects on the mechanical response of the optic nerve head. *Biomech Model Mechanobiol*. 2013;12:941–963.
12. Coudrillier B, Campbell IC, Read AT, et al. Effects of peripapillary scleral stiffening on the deformation of the lamina cribrosa. *Invest Ophthalmol Vis Sci*. 2016;57:2666–2677.
13. Grytz R, Meschke G, Jonas JB. The collagen fibril architecture in the lamina cribrosa and peripapillary sclera predicted by a computational remodeling approach. *Biomech Model Mechanobiol*. 2011;10:371–382.
14. Girard MJ, Suh JK, Bottlang M, Burgoyne CF, Downs JC. Scleral biomechanics in the aging monkey eye. *Invest Ophthalmol Vis Sci*. 2009;50:5226–5237.
15. Coudrillier B, Tian J, Alexander S, Myers KM, Quigley HA, Nguyen TD. Biomechanics of the human posterior sclera: age- and glaucoma-related changes measured using inflation testing. *Invest Ophthalmol Vis Sci*. 2012;53:1714–1728.
16. Fazio MA, Grytz R, Morris JS, et al. Age-related changes in human peripapillary scleral strain. *Biomech Model Mechanobiol*. 2014;13:551–563.
17. Grytz R, Fazio MA, Libertiaux V, et al. Age- and race-related differences in human scleral material properties. *Invest Ophthalmol Vis Sci*. 2014;55:8163–8172.
18. Fazio MA, Grytz R, Morris JS, Bruno L, Girkin CA, Downs JC. Human scleral structural stiffness increases more rapidly with age in donors of African descent compared to donors of European descent. *Invest Ophthalmol Vis Sci*. 2014;55:7189–7198.
19. Girard MJ, Suh JK, Bottlang M, Burgoyne CF, Downs JC. Biomechanical changes in the sclera of monkey eyes exposed to chronic IOP elevations. *Invest Ophthalmol Vis Sci*. 2011;52:5656–5669.
20. Downs JC, Blidner RA, Bellezza AJ, Thompson HW, Hart RT, Burgoyne CF. Peripapillary scleral thickness in perfusion-fixed normal monkey eyes. *Invest Ophthalmol Vis Sci*. 2002;43:2229–2235.
21. Downs JC, Yang H, Girkin C, et al. Three-dimensional histomorphometry of the normal and early glaucomatous monkey optic nerve head: neural canal and subarachnoid space architecture. *Invest Ophthalmol Vis Sci*. 2007;48:3195–3208.
22. Roberts MD, Grau V, Grimm J, et al. Remodeling of the connective tissue microarchitecture of the lamina cribrosa in early experimental glaucoma. *Invest Ophthalmol Vis Sci*. 2009;50:681–690.
23. Yang H, Downs JC, Girkin C, et al. 3-D histomorphometry of the normal and early glaucomatous monkey optic nerve head:

lamina cribrosa and peripapillary scleral position and thickness. *Invest Ophthalmol Vis Sci*. 2007;48:4597–4607.

24. Yang H, Thompson H, Roberts MD, Sigal IA, Downs JC, Burgoyne CF. Deformation of the early glaucomatous monkey optic nerve head connective tissue after acute IOP elevation in 3-D histomorphometric reconstructions. *Invest Ophthalmol Vis Sci*. 2011;52:345–363.
25. Downs JC, Ensor ME, Bellezza AJ, Thompson HW, Hart RT, Burgoyne CF. Posterior scleral thickness in perfusion-fixed normal and early-glaucoma monkey eyes. *Invest Ophthalmol Vis Sci*. 2001;42:3202–3208.
26. Yang H, Qi J, Hardin C, et al. Spectral-domain optical coherence tomography enhanced depth imaging of the normal and glaucomatous nonhuman primate optic nerve head. *Invest Ophthalmol Vis Sci*. 2012;53:394–405.
27. Ivers KM, Sredar N, Patel NB, et al. In vivo changes in lamina cribrosa microarchitecture and optic nerve head structure in early experimental glaucoma. *PLoS One*. 2015;10:e0134223.
28. Ivers KM, Yang H, Gardiner SK, et al. In vivo detection of laminar and peripapillary scleral hypercompliance in early monkey experimental glaucoma. *Invest Ophthalmol Vis Sci*. 2016;57:OCT388–OCT403.
29. Strouthidis NG, Fortune B, Yang H, Sigal IA, Burgoyne CF. Longitudinal change detected by spectral domain optical coherence tomography in the optic nerve head and peripapillary retina in experimental glaucoma. *Invest Ophthalmol Vis Sci*. 2011;52:1206–1219.
30. Downs JC, Roberts MD, Sigal IA. Glaucomatous cupping of the lamina cribrosa: a review of the evidence for active progressive remodeling as a mechanism. *Exp Eye Res*. 2011; 93:133–140.
31. Downs JC, Suh JK, Thomas KA, Bellezza AJ, Hart RT, Burgoyne CF. Viscoelastic material properties of the peripapillary sclera in normal and early-glaucoma monkey eyes. *Invest Ophthalmol Vis Sci*. 2005;46:540–546.
32. Fazio MA, Bruno L, Reynaud JF, Poggialini A, Downs JC. Compensation method for obtaining accurate, sub-micrometer displacement measurements of immersed specimens using electronic speckle interferometry. *Biomed Opt Express*. 2012; 3:407–417.
33. Fazio MA, Grytz R, Bruno L, et al. Regional variations in mechanical strain in the posterior human sclera. *Invest Ophthalmol Vis Sci*. 2012;53:5326–5333.
34. Yang H, Downs JC, Bellezza A, Thompson H, Burgoyne CF. 3-D histomorphometry of the normal and early glaucomatous monkey optic nerve head: prelaminar neural tissues and cupping. *Invest Ophthalmol Vis Sci*. 2007;48:5068–5084.
35. Burgoyne CF, Downs JC, Bellezza AJ, Hart RT. Three-dimensional reconstruction of normal and early glaucoma monkey optic nerve head connective tissues. *Invest Ophthalmol Vis Sci*. 2004;45:4388–4399.
36. See JL, Nicolela MT, Chauhan BC. Rates of neuroretinal rim and peripapillary atrophy area change: a comparative study of glaucoma patients and normal controls. *Ophthalmology*. 2009;116:840–847.
37. Bruno L. Global approach for fitting 2D interferometric data. *Opt Express*. 2007;15:4835–4847.
38. Tang J, Liu J. Ultrasonic measurement of scleral cross-sectional strains during elevations of intraocular pressure: method validation and initial results in posterior porcine sclera. *J Biomech Eng*. 2012;134:091007.
39. Yamaoka A, Matsuo T, Shiraga F, Ohtsuki H. TIMP-1 production by human scleral fibroblast decreases in response to cyclic mechanical stretching. *Ophthalmic Res*. 2001;33: 98–101.
40. Shelton L, Rada JS. Effects of cyclic mechanical stretch on extracellular matrix synthesis by human scleral fibroblasts. *Exp Eye Res*. 2007;84:314–322.
41. Burgoyne CF, Quigley HA, Thompson HW, Vitale S, Varma R. Early changes in optic disc compliance and surface position in experimental glaucoma. *Ophthalmology*. 1995;102:1800–1809.
42. Roberts MD, Sigal IA, Liang Y, Burgoyne CF, Downs JC. Changes in the biomechanical response of the optic nerve head in early experimental glaucoma. *Invest Ophthalmol Vis Sci*. 2010;51:5675–5684.
43. Reeves ND, Maganaris CN, Narici MV. Effect of strength training on human patella tendon mechanical properties of older individuals. *J Physiol*. 2003;548:971–981.
44. Reeves ND. Adaptation of the tendon to mechanical usage. *J Musculoskelet Neuronal Interact*. 2006;6:174–180.
45. Seynnes OR, Koesters A, Gimpl M, et al. Effect of alpine skiing training on tendon mechanical properties in older men and women. *Scand J Med Sci Sports*. 2011;21(suppl 1):39–46.
46. Kubo K, Kanehisa H, Ito M, Fukunaga T. Effects of isometric training on the elasticity of human tendon structures in vivo. *J Appl Physiol (1985)*. 2001;91:26–32.
47. Saeidi N, Sander EA, Ruberti JW. Dynamic shear-influenced collagen self-assembly. *Biomaterials*. 2009;30:6581–6592.
48. Saeidi N, Sander EA, Zareian R, Ruberti JW. Production of highly aligned collagen lamellae by combining shear force and thin film confinement. *Acta Biomater*. 2011;7:2437–2447.
49. Ruberti JW, Hallab NJ. Strain-controlled enzymatic cleavage of collagen in loaded matrix. *Biochem Biophys Res Commun*. 2005;336:483–489.
50. Camp RJ, Liles M, Beale J, et al. Molecular mechanochemistry: low force switch slows enzymatic cleavage of human type I collagen monomer. *J Am Chem Soc*. 2011;133:4073–4078.
51. Chang SW, Flynn BP, Ruberti JW, Buehler MJ. Molecular mechanism of force induced stabilization of collagen against enzymatic breakdown. *Biomaterials*. 2012;33:3852–3859.
52. Flynn BP, Bhole AP, Saeidi N, Liles M, Dimarzio CA, Ruberti JW. Mechanical strain stabilizes reconstituted collagen fibrils against enzymatic degradation by mammalian collagenase matrix metalloproteinase 8 (MMP-8). *PLoS One*. 2010;5: e12337.
53. Flynn BP, Tilburey GE, Ruberti JW. Highly sensitive single-fibril erosion assay demonstrates mechanochemical switch in native collagen fibrils. *Biomech Model Mechanobiol*. 2013; 12:291–300.
54. Hadi MF, Sander EA, Ruberti JW, Barocas VH. Simulated remodeling of loaded collagen networks via strain-dependent enzymatic degradation and constant-rate fiber growth. *Mech Mater*. 2012;44:72–82.
55. Quigley HA, Brown A, Dorman-Pease ME. Alterations in elastin of the optic nerve head in human and experimental glaucoma. *Br J Ophthalmol*. 1991;75:552–557.
56. Quigley HA, Dorman-Pease ME, Brown AE. Quantitative study of collagen and elastin of the optic nerve head and sclera in human and experimental monkey glaucoma. *Curr Eye Res*. 1991;10:877–888.
57. Hernandez MR. Ultrastructural immunocytochemical analysis of elastin in the human lamina cribrosa. Changes in elastic fibers in primary open-angle glaucoma. *Invest Ophthalmol Vis Sci*. 1992;33:2891–2903.
58. Hernandez MR, Andrzejewska WM, Neufeld AH. Changes in the extracellular matrix of the human optic nerve head in primary open-angle glaucoma. *Am J Ophthalmol*. 1990;109: 180–188.
59. Hernandez MR, Ye H. Glaucoma: changes in extracellular matrix in the optic nerve head. *Ann Med*. 1993;25:309–315.
60. Strouthidis NG, Girard MJ. Altering the way the optic nerve head responds to intraocular pressure-a potential approach to glaucoma therapy. *Curr Opin Pharmacol*. 2013;13:83–89.

Investigative Ophthalmology & Visual Science

61. Tielsch JM, Sommer A, Katz J, Royall RM, Quigley HA, Javitt J. Racial variations in the prevalence of primary open-angle glaucoma. The Baltimore Eye Survey. *JAMA*. 1991;266:369–374.
62. Friedman DS, Wolfs RC, O'Colmain BJ, et al. Prevalence of open-angle glaucoma among adults in the United States. *Arch Ophthalmol*. 2004;122:532–538.
63. Tham YC, Li X, Wong TY, Quigley HA, Aung T, Cheng CY. Global prevalence of glaucoma and projections of glaucoma burden through 2040: a systematic review and meta-analysis. *Ophthalmology*. 2014;121:2081–2090.
64. Cone-Kimball E, Nguyen C, Oglesby EN, Pease ME, Steinhart MR, Quigley HA. Scleral structural alterations associated with chronic experimental intraocular pressure elevation in mice. *Mol Vis*. 2013;19:2023–2039.
65. Nguyen C, Cone FE, Nguyen TD, et al. Studies of scleral biomechanical behavior related to susceptibility for retinal ganglion cell loss in experimental mouse glaucoma. *Invest Ophthalmol Vis Sci*. 2013;54:1767–1780.
66. Turner DC, Edmiston AM, Zohner YE, et al. Transient intraocular pressure fluctuations: source, magnitude, frequency, and associated mechanical energy. *Invest Ophthalmol Vis Sci*. 2019;60:2572–2582.
67. Markert JE, Jasien JV, Turner DC, Huisingh C, Girkin CA, Downs JC. IOP, IOP transient impulse, ocular perfusion pressure, and mean arterial pressure relationships in nonhuman primates instrumented with telemetry. *Invest Ophthalmol Vis Sci*. 2018;59:4496–4505.
68. Jasien JV, Turner DC, Girkin CA, Downs JC. Cyclic pattern of intraocular pressure (IOP) and transient IOP fluctuations in nonhuman primates measured with continuous wireless telemetry. *Curr Eye Res*. 2019;19:1–9.
69. Girard MJ, Downs JC, Bottlang M, Burgoyne CF, Suh JK. Peripapillary and posterior scleral mechanics–part II: experimental and inverse finite element characterization. *J Biomech Eng*. 2009;131:051012.
70. Girard MJ, Downs JC, Burgoyne CF, Suh JK. Peripapillary and posterior scleral mechanics–part I: development of an anisotropic hyperelastic constitutive model. *J Biomech Eng*. 2009;131:051011.
71. Ollivier FJ, Brooks DE, Kallberg ME, et al. Time-specific intraocular pressure curves in Rhesus macaques (Macaca mulatta) with laser-induced ocular hypertension. *Vet Ophthalmol*. 2004;7:23–27.
72. Downs JC. IOP telemetry in the nonhuman primate. *Exp Eye Res*. 2015;141:91–98.
73. Downs JC, Burgoyne CF, Seigfreid WP, Reynaud JF, Strouthidis NG, Sallee V. 24-hour IOP telemetry in the nonhuman primate: implant system performance and initial characterization of IOP at multiple timescales. *Invest Ophthalmol Vis Sci*. 2011;52:7365–7375.

Investigative Ophthalmology & Visual Science